Photophysical Properties of Tyrosine and Its Simple Derivatives Studied by Time-Resolved Fluorescence Spectroscopy, Global Analysis, and Theoretical Calculations

Katarzyna Guzow,[†] Robert Ganzynkowicz,[†] Alicja Rzeska,[†] Justyna Mrozek,[†] Mariusz Szabelski,[†] Jerzy Karolczak,[‡] Adam Liwo,[†] and Wiesław Wiczk*[,†]

Faculty of Chemistry, University of Gdańsk, Sobieskiego 18, 80-952 Gdańsk, Poland, and Quantum Electronics Laboratory, Faculty of Physics, Adam Mickiewicz University, Umultowska 85, 61-614 Poznań, Poland

Received: September 12, 2003; In Final Form: January 9, 2004

The photophysical properties of tyrosine and its derivatives with free and blocked functional groups in water were studied by steady-state and time-resolved fluorescence spectroscopy and global analysis. Tyrosine fluorescence intensity decays in water at pH = 5.5 in the short-wavelength region (290−320 nm) are monoexponential, whereas, at longer wavelengths, they are biexponential. The monoexponential fluorescence intensity decay of *O*-methyl tyrosine across the fluorescence band is observed. The fluorescence lifetimes of Tyr calculated using a global analysis are equal to 3.37 ± 0.04 ns at the short-wavelength region and 0.98 ± 0.12 ns at the longer-wavelength region. This observation, together with the decay-associated spectra, indicate that the short-lifetime component can be attributed to tyrosine with phenol hydroxyl groups hydrogen-bonded with water molecules. The rotamer populations calculated from potentials of mean forces, as well as those obtained from ^{1}H NMR spectroscopy, do not correspond to the pre-exponential factors obtained from fluorescence spectroscopy. The calculated energy barriers of rotations about the $C^{\alpha}-C^{\beta}$ bond indicate that the interconversion rate constant for tyrosine and *N*-acetyl-tyrosinamide are much greater than the fluorescence rate constant. Monoexponential fluorescence intensity decay of tyrosine derivatives in acetonitrile solution is observed for all derivatives studied and, contrary to the aqueous solution, the amide group does not quench the fluorescence. Thus, specific conformation(s) stabilized by the hydrogen-bond network seem to be responsible for the heterogeneous fluorescence intensity decay of tyrosine derivatives in aqueous solution.

1. Introduction

The fluorescence of aromatic amino acids (phenylalanine, tyrosine, and tryptophan) and their residues, incorporated into a peptide or protein chain, is a subject of extensive studies, because of the use of such materials as internal probes in conformational analysis.[1−3] In the case of the tyrosine zwitterion and tyrosine derivatives with an ionized α-carboxyl group, monoexponential fluorescence decays were observed.[3−8] The conversion of the α-carboxyl group into the corresponding amide or its protonation results in a complex fluorescence decay.[1−8] Some explanation of this behavior was offered by the Gauduchon and Whal ground-state rotamer model.[6] This model assumes the existence of well-defined ground-state $C^{\alpha}-C^{\beta}$ bond rotamers, where interconversion time is considerably longer than the excited-state lifetimes of the rotamers. This rotamer model has been further extended to the $C^{\beta}-C^{\gamma}$ bond conformers.[9−12] The different lifetimes of the rotamers result from the interaction between the phenol fluorophore and the quenching groups. The quenching efficiency is controlled by the orientation of both groups and is dependent on distance.[13,14] Cowgill,[15,16] Tournon et al.,[17] and Feitelson[18] suggested that the fluorescence quenching of an aromatic amino acid side chain by the peptide (amide) group occurred because of a charge transfer between the excited aromatic chromophore (phenol ring), acting as a donor, and electrophilic units in the amino acid backbone (the carbonyl of the amide group), acting as an acceptor. Such a mechanism of the fluorescence quenching of tyrosine by amide groups was further supported by the dependence of quenching efficiency on the distance between the phenol group of tyrosine residue and the amide group, and the type of the substituent on the N amide atom,[13,14] as well as by the parabolic relation of the logarithm of electron-transfer rate constant from the aromatic portion to the amide group to the ionization potential of aromatic amino acids.[7]

In the case of tyrosine analogues and derivatives, the rotamer model showed that the rotamer in which the phenol ring can come into the closest contact with the carbonyl group had the shortest fluorescence lifetime. Because of slow rotamer interconversion, the rotamer model predicts that the fluorescence intensity decay should be described by a sum of three exponentials terms. For those tyrosine derivatives that exhibit a monoexponential or biexponential decay, it is assumed that the three or two rotamers have similar unresolved fluorescence lifetimes or rotamer interconversion is fast, averaging the emission.[3−5] However, based on the ground-state rotamer model, the photophysical properties of simple tyrosine derivatives or analogues (β-Tyr(Me),[19] β-Hty,[20] Phg(OH),[21] and Tic(OH)[22]) could not be fully explained. The acetylation of the amino group of tyrosine or its analogues causes moderate decrease of the fluorescence quantum yield and the fluorescence lifetime; however, the fluorescence intensity decay is still monoexponential.[3] The methylation of the hydroxyl group of the phenolic ring of tyrosine increases both the fluorescence quantum yield and the fluorescence lifetime, in comparison to those of tyrosine,

* Author to whom correspondence should be addressed. E-mail: ww@chem.univ.gda.pl.
[†] University of Gdańsk.
[‡] Adam Mickiewicz University.

10.1021/jp036721c CCC: $27.50
Published on Web 03/02/2004

but it does not change the character of the fluorescence intensity decay of tyrosine itself, its amide, or its *N*-acetyl derivatives.[3,14]

The photophysical properties of buried tyrosine residues in proteins are different than those of tyrosine that has been exposed to the solvent.[23] They also undergo substantial changes while the protein folds from a random coil to a globular structure.[24] To explain the photophysical properties of tyrosine and the influence of substituents on the amino and carboxyl group on the photophysical properties in water and acetonitrile, the obtained experimental results are discussed based on theoretical calculations of the rotamer populations and the rate of interconversion between them. The rate constant of rotamer interconversion, as well as the rotamer population, were estimated from the respective potential of mean force (PMF), which is determined by the umbrella-sampling molecular dynamics (MD) method.[25−29]

2. Materials and Methods

Tyrosine (Tyr), *N*-acetyl-tyrosine (AcTyr), *N*-acetyl-tyrosinamide ($AcTyrNH_2$), and *O*-methyl-tyrosine (Tyr(Me)) were obtained from Aldrich. *N*-acetyl-*O*-methyl-tyrosine methyl ester (AcTyr(Me)OMe) and *N*-*tert*-butyloxycarbonyl-*O*-methyl tyrosine (BocTyr(Me)) were purchased from Bachem. Water was purified using the Milli-Q sytem (Millipore). Acetonitrile for high-performance liquid chromatography (HPLC) was obtained from LabScan, whereas HCl ("Suprapur", 30% solution) was obtained from Merck. All compounds were used without additional purification, after their purity was checked using analytical high-performance reversed-phase liquid chromatography (RP−HPLC).

2.1. Synthesis. 2.1.1. Synthesis of *N*-Acetyl-*O*-methyl-tyrosine (AcTyr(Me)). *N*-Acetyl-*O*-methyl-tyrosine was obtained from AcTyr(Me)OMe by saponification, according to the literature procedure.[30]

2.1.2. Synthesis of *N*-Acetyl-*O*-methyl-tyrosinamide ($AcTyr(Me)NH_2$). *N*-Acetyl-*O*-methyl-tyrosinamide was obtained from AcTyr(Me)OMe by ammonolysis, according to the literature procedure.[30]

2.1.3. Synthesis of *O*-Methyl-tyrosinamide ($Tyr(Me)NH_2$). *O*-Methyl-tyrosinamide ($Tyr(Me)NH_2$) was synthesized using BocTyr(Me), by applying a mixed anhydride method, followed by the removal of the Boc-protecting group, using trifluoroacetic acid/methylene chloride (50% v/v).[30]

All prepared derivatives were purified by RP−HPLC, and the chemical purity of all compounds studied was assessed by analytical RP−HPLC and mass spectrometry (field desorption (FD) or fast atom bombardment (FAB)). The structure of all synthesized compounds was confirmed by Fourier transform infrared (FTIR) and ^{1}H nuclear magnetic resonance (NMR) analyses.

2.2. Spectroscopic Measurements. The absorption spectra of tyrosine and its studied derivatives were recorded on a spectrophotometer (Perkin−Elmer, model Lambda-18).

The emission spectra were recorded using a spectrofluorimeter (Perkin−Elmer, model LS-50B). The quantum yields of tyrosine and its derivatives were obtained by comparing the integral intensity of the steady-state emission spectra that were excited at 275 nm (corrected for absorbance) with that of tyrosine in water, using a value of 0.14 for the latter.[31] The optical density of the sample at this excitation wavelength did not exceed 0.1, and the monochromator band-pass was set to 2.5 nm in both the excitation and emission sides.

2.3. Time-Resolved Fluorescence Measurements. The fluorescence intensity decays were measured using the time-correlated single-photon counting apparatus at the Centre for Ultrafast Laser Spectroscopy, Adam Mickiewicz University (Poznań, Poland). The excitation source ($\lambda_{ex} = 277$ nm) was a picosecond/femtosecond laser system (Ti:Sapphire "Tsunami" laser, pumped with an Ar^+ ion laser "BeamLok" 2060 and equipped with a cooled photomultiplier tube (model 3809U-05 MCP)). The half-width of the instrument response function was ~35 ps.[32] All fluorescence measurements were performed with the emission polarizer set at 54.7°, with respect to the excitation polarization. The channel width (δt) was set to 48.8 ps/ch in all measurements, except for tyrosine amide derivatives in water for which δt was 24.4 ps/ch. The desired emission wavelength was selected using a monochromator ($\Delta\lambda = 4.8$ nm). A Ludox solution was used to collect the instrument response. Fluorescence decays for the sample and reference were measured to 1×10^4 and 4×10^4 counts in the channel, respectively. All measurements were performed at 20 °C at pH = 5.5 adjusted using a HCl solution. The fluorescence decay data were fitted by the iterative convolution to the sum of the exponents:

$$I(\lambda,t) = \sum_i \alpha_i(\lambda) \exp\left(-\frac{t}{\tau_i}\right) \quad (1)$$

where τ_i is the decay time of the *i*th component and $\alpha_i(\lambda)$ is its pre-exponential factor at the emission wavelength λ.

This model assumes that τ_i is independent of λ; therefore, the decay curves, which have been taken at different emission wavelengths, can be analyzed simultaneously.[33,34] The data were analyzed by a global least-squares iterative convolution program that was supplied by Edinburgh Analytical Instruments (FLA-900 Level 2 software). The adequacy of the exponential decay fitting was judged by the inspection of the plots of weighted residuals and by the statistical parameters χ^2_R and the shape of the autocorrelation function of the weighted residuals and serial variance ratio (SVR). In all cases, the fitting was started at the peak channel of the response function. The fluorescence lifetime errors presented in this work were calculated as asymptotic errors by the software used.

Decay-associated spectra (DAS), which are the emission spectra associated with each individual decay component,[35,36] were calculated from eq 2:

$$I_i(\lambda) = I_{SS}(\lambda)\left(\frac{\alpha_i(\lambda)\tau_i}{\sum_i \alpha_i(\lambda)\tau_i}\right) \quad (2)$$

where $I_i(\lambda)$ is the emission spectrum associated with the *i*th component and I_{SS} is the total steady-state spectrum.

2.4. ^{1}H NMR Measurements. ^{1}H NMR spectra of tyrosine and its derivatives were recorded using a Varian Unity Plus 500 MHz instrument in D_2O. All ^{1}H NMR spectra were obtained at 20 °C in the pulse and Fourier transform mode, and the coupling constants were obtained with an estimated accuracy of ±0.2 Hz. For $AcTyrNH_2$, ^{1}H NMR spectra were recorded in the temperature range of 20−80 °C, with a step of 10 °C. The fractional populations p_I, p_{II}, and p_{III} of rotamers I, II, and III, respectively, that were associated with the rotation about the $C^\alpha-C^\beta$ bond (the χ_1 rotamers assigned according to Laws et al.[5]) were calculated from the coupling constants between vicinal

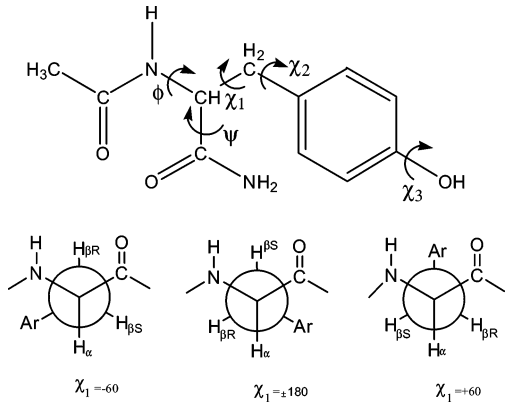

Figure 1. Designation of dihedral angles in tyrosine derivatives (top) and Newman projection about the $C^{\alpha}-C^{\beta}$ bond (bottom).

H^{α} and $H^{\beta R}$ ($H^{\beta S}$) using following equations:

$$p_{\mathrm{I}} = \frac{{}^3J(H^{\alpha} - H^{\beta R}) - {}^3J_{\mathrm{g}}}{\Delta^3 J} \tag{3a}$$

$$p_{\mathrm{II}} = \frac{{}^3J(H^{\alpha} - H^{\beta S}) - {}^3J_{\mathrm{g}}}{\Delta^3 J} \tag{3b}$$

$$p_{\mathrm{III}} = 1 - p_{\mathrm{I}} - p_{\mathrm{II}} \tag{3c}$$

where $\Delta^3 J = {}^3J_{\mathrm{t}} - {}^3J_{\mathrm{g}}$, and ${}^3J_{\mathrm{t}} = 13.56$ Hz and ${}^3J_{\mathrm{g}} = 2.6$ Hz are the nominal values of the coupling constants for vicinal protons in trans and gauche conformations, respectively.[5]

2.5. Theoretical Calculations. One fundamental measure of the effective interactions between solute molecules in solution is the potential of mean force (PMF), i.e., the free energy as a function of the configuration of the solute. In this work, the PMF profiles were expressed as functions of single dihedral angles (χ_1, χ_2, χ_3, φ, or ψ), which are defined in Figure 1. Each PMF is defined by eq 4:

$$W(\theta) = -RT \ln P(\theta,T,V) \tag{4}$$

where $P(\theta)$ is the probability density of the angle of interest (θ) for a given pressure p, temperature T, and volume V of the system, as expressed by eq 5:

$$P(\theta,T,V) = \frac{\int_{\Omega_\theta} \exp[(-H(x))/(RT)]\, \mathrm{d}\Omega_\theta}{\int_{\Omega} \exp[(-H(x))/(RT)]\, \mathrm{d}\Omega} \tag{5}$$

where H is the Hamiltonian of the system (solute plus solvent), x denotes all degrees of freedom of the solute and the solvent, V denotes the entire configuration space of the system, and Ω_θ is the configurational space of the system restricted to a given angle θ.

To determine the PMF by molecular simulations, we used the umbrella-sampling method.[37,38] We imposed a series of restraining potentials V on the reaction coordinate to ensure that all regions are sampled sufficiently. Each restraint defined a sampling window. The total Hamiltonian of the system (including the restraining potential) for the ith window was defined by

$$H_i(\theta) = V_0(\theta) + V_i(\theta) = V_0(\theta) + \frac{1}{2}K_i[\mathrm{mod}(\theta - \theta^0, 2\pi)]^2 \tag{6}$$

where $V_0(\theta)$ is the energy function of the system that consists of the solute and the solvent, K_i is the force constant of the restraining potential, and θ_i^0 is the equilibrium angle of the restraining potential; we assumed a value of $K = 2.0$ kcal/(mol Å^2)$^{-1}$ and we assumed that 13 windows with θ varying from $-180°$ to 180°, in increments of 30°, were used. To calculate the PMF from umbrella-sampling simulation data, we used the weighted histogram analysis method (WHAM).[26−28] This method processes the results of simulations from all windows simultaneously and removes the contribution due to the restraining potentials V_i. MD simulations were performed to sample the configurations corresponding to each window.

The simulations were conducted in the NVT scheme with the AMBER 5.0[39] force field and the TIP3P model of water.[40,41] Calculations were performed using a cubic periodic box with sides 20 Å long. A 7-Å cutoff and an 8-Å second cutoff were applied, to control the nonbonded interaction, except electrostatic interactions that follows on the parametrization.[40,41] Consequently, the minimum-image convention, according to which the cutoff on nonbonded interactions should not exceed half of the box size, which prevents the molecule studied from interacting with its images, was applied. The duration of simulation in each window was 1 ns and the sampling frequency was 2 fs. The bin size in counting the occurrence of the dihedral angle of interest was 5°.

Electrostatic energy was evaluated using the particle-mesh Ewald summation.[41] The force-field parameters of tyrosine were taken from the AMBER database.[39] According to the rotamer theory,[3−6] the heterogeneity of the fluorescence intensity decay of tyrosine derivatives is determined by the population of ground-state rotamers, which do not interconvert during the excited-state lifetime of fluorophores. Therefore, we did not derive additional force fields for the tyrosine derivatives studied in the excited state, nor did we use them any further. To check the accuracy of the derived PMF curves, we evaluated the PMF without symmetry constrains, even for those dihedral angles for which the PMF surface should be symmetric (the χ_2, χ_3, φ, and ψ angles of tyrosine). The deviation of the resulting PMF curves from 2-fold or 3-fold symmetry, respectively, were <0.1 kcal/mol, which demonstrates that the sampling was sufficient (see Table 5 later in this paper).

The PMF was used to calculate the relative rotamer population (p_i) by applying eqs 7 and 8:

$$z_i = \int_{\theta_1^i}^{\theta_2^i} \exp\left(-\frac{\mathrm{PMF}(\theta)}{RT}\right) \mathrm{d}\theta \tag{7}$$

$$p_i = \frac{z_i}{\sum_i z_i} \tag{8}$$

where R is the gas constant and T is the absolute temperature.

The rate of rotamer interconversion ($k_{\mathrm{rot1}\rightarrow\mathrm{rot2}}$) was estimated from transition-state theory:[22]

$$k_{\mathrm{rot1}\rightarrow\mathrm{rot2}} = \kappa\left(\frac{kT}{h}\right) \exp\left(-\frac{\Delta\mathrm{PMF}}{RT}\right) \tag{9}$$

where κ is the transition coefficient, k is the Boltzmann constant, h is Planck's constant, and ΔPMF is the difference between a minimal and maximal values of PMF (i.e., the free energy of activations). It is difficult to assign a value to the transition coefficient (κ), which incorporates all correction factors and uncertainties. Using stochastic MD simulations, Kuharski et al.[42]

TABLE 1: Fluorescence Lifetime (τ), Pre-exponential Factor (α), and Quality of Fit (χ^2_R)[a] for Tyrosine (Tyr) and *O*-Methyl Tyrosine (Tyr(Me)) in Water at Different Observation Wavelengths

	Tyr			Tyr(Me)		
λ_{em} (nm)	τ_i (ns)	α_i	χ^2_R	τ (ns)	α	χ^2_R
285				4.82	1	1.12
290	3.39	1	1.12	4.83	1	1.14
300	3.4	1	1.11	4.82	1	1.13
310	3.4	1	1.14	4.84	1	1.07
315				4.82	1	1.14
320	3.37	1	1.13	4.83	1	1.02
330	3.31	1.000	2.59	4.81	1	1.14
	3.55; 1.43	0.756; 0.244	1.14			
340	3.90	1.000	7.46	4.85	1	1.11
	3.83; 1.38	0.500; 0.500	1.10			
350	3.05	1.000	14.2	4.82	1.000	1.41
	4.17; 1.27	0.607; 0.393	1.19	4.95; 1.75	0.889; 0.112	1.07
	2.99; 0.85; 6.01	0.443; 0.473; 0.084	1.04			
360	3.75	1.000	12.7	4.85	1.000	4.72
	4.36; 1.35	0.507; 0.493	1.18	4.91; 1.67	0.863; 0.137	1.10
	2.84; 0.81; 6.67	0.407; 0.43; 0.160	1.06			
370	3.54	1.000	10.2	4.79	1.000	6.03
	4.55; 1.30	0.431; 0.569	1.18	5.04; 1.97	0.820; 0.180	1.12
	2.966; 0.77; 5.47	0.398; 0.391; 0.211	1.00			

[a] For one, two, and three components, respectively.

computed a value of 0.4 for cyclohexane isomerization in a low viscosity; therefore, we chose $\kappa = 1$ for a single bond rotation. Note that eq 9 provides only a crude estimate of the interconversion rate, because it neglects the friction and stochastic forces. These could be accounted only in direct MD simulations of the interconversion process, which are, however, infeasible, because the time scale is too large.

3. Results and Discussion

3.1. Tyrosine and *O*-Methyl-tyrosine Emission in Water at pH = 5.5. 3.1.1. Steady-State Fluorescence Spectroscopy. The absorption and emission spectra of Tyr and Tyr(Me) in water at pH = 5.5 are very similar to those of $AcTyrNH_2$ and $AcTyr(Me)NH_2$, as well as to the published spectra. Methylation of the hydroxyl group of tyrosine causes a small (~1−2 nm) blue-shift of both the absorption and fluorescence spectra, compared to that of Tyr, and substantially increases the fluorescence quantum yield (0.201 for Tyr(Me),[7,14,31] compared to 0.14 for Tyr; see Table 3 later in this paper).

3.1.2. Time-Resolved Fluorescence Spectroscopy. The fluorescence intensity decays in water at pH = 5.5 for Tyr, as well as the fluorescence intensity decay of impurities in the water, were measured at 9 different observation wavelengths in the range of 290−370 nm, whereas for Tyr(Me), the decays were measured at 11 wavelengths (285−370 nm). In the short-wavelength region (290−320 nm), the fluorescence intensity decays of Tyr are monoexponential, whereas they are heterogeneous for the longer observation wavelengths (see Table 1 and Figure 2). For an adequate description of the Tyr fluorescence intensity decays recorded at 330 and 340 nm, two exponents were needed, whereas for longer observation wavelengths (350, 360, and 370 nm), functions in the form of a sum of three exponents gave acceptable values of χ^2_R. In the case of Tyr(Me), the monoexponential fluorescence intensity decays were observed up to 340 nm. For longer observation wavelengths (350, 360, and 370 nm), the fluorescence intensity decays were heterogeneous and the heterogeneity, measured as a deviation from the monoexponential decay (χ^2_R values), increased as the observation wavelength increased (see Table 1).

The obtained data for the Tyr fluorescence intensity decays were globally analyzed, assuming different fluorescence decay models, with either one, two, or three fluorescence lifetimes used as free or global parameters. The global analysis of the fluorescence decay curves of Tyr, with an assumption of the monoexponential decay function and the fluorescence lifetime as a free parameter, gave an unacceptably high value of χ^2_R (5.55); however, when the fluorescence lifetime was a global parameter (the same for all data sets), the χ^2_R value increased to 6.59. The fit of a biexponential function with two nonglobal lifetimes gave a value of $\chi^2_R = 1.16$. The global fit of the biexponential function with two fluorescence decay times—one

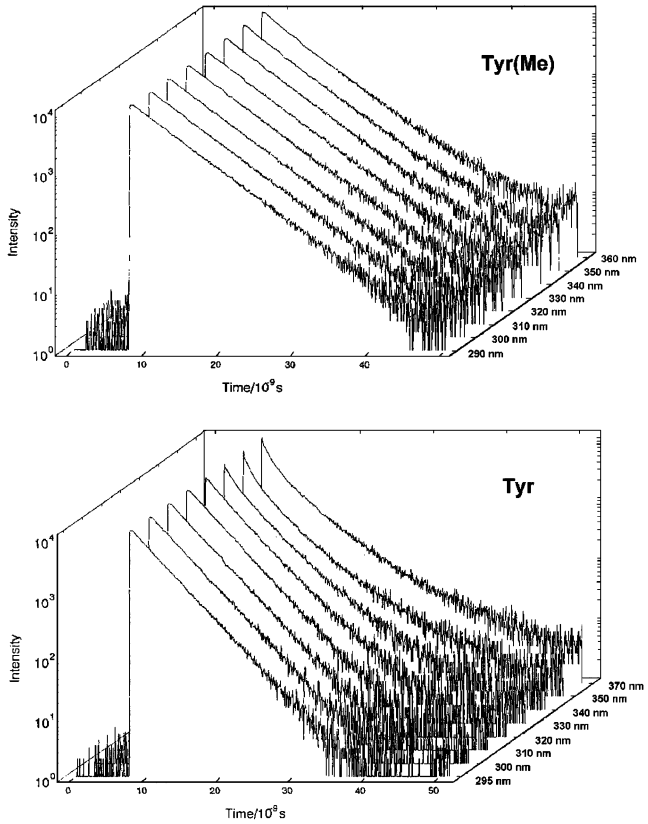

Figure 2. Fluorescence intensity decays of *O*-methyl tyrosine (Tyr(Me), top) and tyrosine (Tyr, bottom) in water at pH = 5.5.

TABLE 2: Pre-exponential Factor (α_i) and the Fractional Contribution (f_i)[a] Obtained from Global Analysis (τ_1 and τ_2 Global Parameters) of Tyrosine Fluorescence Decays in Water at pH = 5.5[b]

	$\tau_1^G = 3.40$ ns		$\tau_2^G = 0.98$ ns					
λ_{em} (nm)	α_1	f_1	α_2	f_2	τ_3	α_3	f_3	χ_R^2
290	0.994	0.998	0.01	0				0.88
300	0.995	0.998	0.01	0				1.01
310	0.988	0.996	0.012	0				1.02
320	0.965	0.99	0.035	0.01				0.97
330	0.775	0.917	0.221	0.08	5.28	0	0	1.03
340	0.586	0.806	0.401	0.159	6.63	0	0.04	1.06
350	0.409	0.688	0.583	0.283	7.39	0	0.03	1.07
360	0.392	0.603	0.562	0.25	7.08	0	0.147	1.06
370	0.386	0.58	0.546	0.237	6.08	0.07	0.183	1.17

[a] $f_i = \alpha_i\tau_i/(\sum_i \alpha_i\tau_i)$. [b] Global $\chi_R^2 = 1.10$.

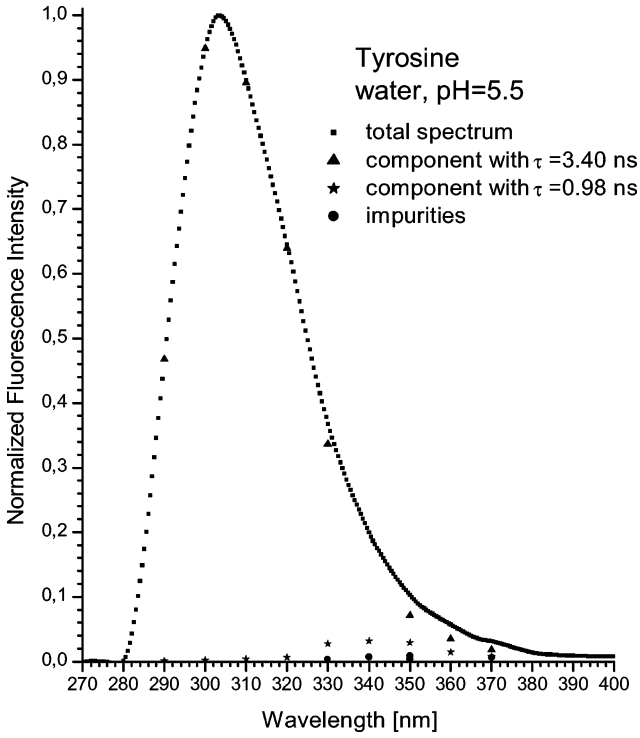

Figure 3. Decay-associated spectra (DAS) of tyrosine in water at pH = 5.5.

common time for all analyzed data sets (global parameters) and a second independent (nonglobal) time and independent pre-exponential factors resulted in slightly higher χ_R^2 values (1.28) than those for the biexponential fit with nonglobal parameters. The χ_R^2 values substantially increased (to 2.26) when both fluorescence lifetimes were the global parameters. The fit of the three-exponential function, with two fluorescence lifetimes as global parameters and a third fluorescence lifetime, and pre-exponential factors as nonglobal parameters to the experimental data set gave a low value of χ_R^2 (1.10) and fluorescence lifetimes equal to 3.37 and 0.98 ns with the pre-exponential factors presented in Table 2. The same value of χ_R^2 was obtained using the three-exponential function with all nonglobal parameters. The longer fluorescence lifetime is very similar to that published previously[3−6,13,20,43−45] for Tyr at short observation wavelengths. Based on eq 2 and the parameters collected in Table 2, the DAS were constructed (Figure 3). The fluorescence spectrum associated with the longer fluorescence lifetime (3.4 ns) conforms to the fluorescence spectrum of Tyr, with a maximum at ∼302 nm, whereas the spectrum associated with the shorter fluorescence lifetime (1 ns) is red-shifted, compared to the previous spectrum, and possesses a maximum at ∼350 nm and is similar to the fluorescence spectrum of tyrosine hydrogen-bonded to the hydrogen acceptor[46−52] or the fluorescence spectrum of tyrosinate.[47] The biexponential fluorescence intensity decay for Tyr and tyrosine residue in a dipeptide at a single observation wavelength (340 nm) was observed by Willis and Szabo[50] and Harms et al.,[53] as well as by Ferreira et al. in a water−glycerol mixture.[54] Taking into account that the fluorescence lifetime of tyrosinate is much shorter (∼30 ps[47,50,55]) than that observed, and that the ionization of the Tyr hydroxyl in water is thermodynamically allowed but kinetically forbidden,[3,5,45,47] it can be assumed that the species with a fluorescence lifetime of ∼1 ns (the spectrum of which is red-shifted, compared to that of Tyr) is tyrosine that has been hydrogen-bonded to the water molecule(s) by its hydrogen group.[50,53] The fluorescence excitation spectra of Tyr measured at 300 and 350 nm (spectra not shown) revealed that the former is the excitation spectrum of tyrosine, whereas the latter is red-shifted by ∼1−2 nm, as it was observed by Lee et al.[51] for Tyr hydrogen-bonded complexes. The third component was observed at longer fluorescence wavelengths (on the tail of the fluorescence spectrum of tyrosine, where the fluorescence intensity of tyrosine is weak), with a small contribution to the fluorescence decay and the fluorescence lifetime was too long, as it was for tyrosine (∼7 ns). The long-lifetime component in the sample decay observed at the long-wavelength fluorescence could be associated with the fluorescence of water impurities, because of the similar fluorescence lifetime of the "solvent" blank (8−10 ns). However, the contribution of photoproduct(s) fluorescence cannot be excluded.[53,56,57]

The global analysis of the fluorescence intensity decays of Tyr(Me) measured under the same conditions as the Tyr fluorescence intensity decay (water at pH = 5.5) reveals that the fluorescence intensity decay is monoexponential. The fit of the monoexponential function with all nonglobal parameters gave a low χ_R^2 value (1.24), which slightly increased to 1.29 when the fluorescence lifetime is a global parameter ($\tau = 4.87$ ns). The fit to the biexponential function with one fluorescence lifetime as a global parameter and all remaining parameters as independent parameters gave a low χ_R^2 value (1.09) and a fluorescence lifetime of $\tau = 4.82$ ns. The second nonglobal fluorescence lifetime is in the range from 1.2 ns to ∼8 ns with a very low contribution (∼1%). The obtained fluorescence decay time of Tyr(Me) is comparable to the published value obtained for single observation wavelength.[3−5,7] The monoexponential fluorescence intensity decay of Tyr(Me) additionally supports the conclusion that the biexponential fluorescence intensity decay of Tyr is caused by the interaction of phenolic hydroxyl with water molecules. The shorter fluorescence lifetime of tyrosine, compared to Tyr with an *O*-methylated hydroxyl group, is caused by the quenching of Tyr fluorescence by water and the quenching action can be attributed to a Tyr−H_2O exciplex.[58]

3.2. Influence of a Substituent on Amino or/and Carboxyl Group on Fluorescence Properties of Tyr and Tyr(Me) in Water. The absorption spectra of Tyr or Tyr(Me) derivatives that possess a substituent(s) on the amino group (AcTyr or AcTyr(Me)), the carboxyl group ($TyrNH_2$ or $Tyr(Me)NH_2$), or both groups ($AcTyrNH_2$ or $AcTyr(Me)NH_2$) are similar to those of the parent molecules; however, the fluorescence intensities of these derivatives are diversified and are dependent on the type of substituent (Table 3). The stronger fluorescence quenching effect is observed for the $TyrNH_2$ and $Tyr(Me)NH_2$ derivatives, compared to the parent molecules, whereas the

TABLE 3: Fluorescence Lifetime (τ) and Quality of Fit (χ^2_R) Obtained from Global Analysis, and the Pre-exponential Factor (α) Obtained from the Single-File Analysis at 315 nm, the Fluorescence Rate Constant (k_f), and the Nonradiative Rate Constant (k_{nr}) for Tyrosine and Its Derivatives in Water at pH = 5.5

τ (ns)	α	χ^2_R	$\langle\tau\rangle^a$ (ns)	k_f ($\times 10^{-7}$ s^{-1})	k_{nr} ($\times 10^{-8}$ s^{-1})
Tyr,[b] QY = 0.14					
3.40 ± 0.04	1	1.06		4.17	2.56
AcTyr, QY = 0.135					
3.23	1.000	1.31			
3.27 ± 0.01	0.881				
0.60 ± 0.08	0.119	1.04	3.22	4.2	2.69
$TyrNH_2$, QY = 0.05					
1.19	1.000	8.67			
1.39 ± 0.01	0.564				
0.43 ± 0.01	0.436	1.10	1.21	4.15	7.88
$AcTyrNH_2$, QY = 0.07					
1.58	1.000	2.82			
1.67 ± 0.01	0.798				
0.40 ± 0.07	0.202	1.07	1.6	4.07	5.85
Tyr(Me), QY = 0.201					
4.82 ± 0.06	1	1.06		4.17	1.66
AcTyr(Me), QY = 0.185					
4.48 ± 0.04	1	1.06		4.13	1.82
$Tyr(Me)NH_2$, QY = 0.06					
1.49	1.000	1.74			
1.52 ± 0.06	0.750				
0.42 ± 0.14	0.250	1.10	1.43	4.06	6.59
$AcTyr(Me)NH_2$, QY = 0.1					
2.43	1	1.26			
2.46 ± 0.03	0.936				
0.66 ± 0.44	0.064	1.02	2.42	4.09	3.72

[a] $\langle\tau\rangle = \alpha_i\tau_i^2/(\sum_i\alpha_i\tau_i)$. [b] Calculated from the fluorescence decays measured for the short-wave region at 310 nm.

introduction of a second substituent (acetylation of the amino group) slightly increases the fluorescence quantum yield. The small quenching effect can be observed for the derivatives that contain only an acetyl group. For AcTyr and AcTyr(Me), the fluorescence quantum yields are 96% and 92% of those of the parent molecule, respectively (see Table 3). A substantial decrease of the fluorescence quantum yield caused by the conversion of the ionized carboxyl group into the amide group was also observed by other workers.[3−6,15,43,59,60] A weaker quenching ability of the fluorescence of the Tyr[3−6,13,43] and tyrosine analogues[19,21,22] by the acetyl group, compared to the amide group, was also observed and is consistent with the statement that the N-terminal portion of a peptide is a weaker quencher of the Tyr fluorescence than its C-terminal portion,[13,60,61] probably because of the difference of redox potential between the N- and C-terminal residues.[62] The fluorescence quantum yield of a tyrosine derivative that possesses two quenching groups (acetyl and amide) is greater than that of a tyrosine amide (one quenching group) with a protonated amino group. The influence of the protonated amino group on the quenching ability of the phenol chromophore by the amide group is dependent on the distance between them.[13,61] These parameters explicitly indicate the important role of the amino group in the neighborhood of the quencher (carbonyl) in the quenching process of the fluorescence of aromatic amino acids. The protonated amino group does not quench the tyramine fluorescence[5,6,8] and is not attributed directly to a straight quenching process of the tyrosine fluorescence,[3,6,8,9,15,63] which has been discussed in terms of electrostatic effect. The electrostatic field produced by the ammonium group in the derivatives of tyrosine with a protected carboxyl group can change the polarization of the surrounding water molecules and will lead to higher polarization of the carbonyl group and an increasing electron-acceptor property of the amide group that is facilitating electron transfer. This hypothesis has been supported by the lower quenching efficiency of the Tyr−Gly dipeptide with the ionized carboxyl group (electron donor), compared to $TyrNH_2$[5,6] and the *N*-methyl-substituted amide group,[14] and the weaker acidity of the carboxyl group of *N*-acetyl tyrosine, compared to tyrosine with a protonated amino group.[64]

3.2.1. Time-Resolved Fluorescence Spectroscopy. The fluorescence intensity decays of Tyr and Tyr(Me) derivatives in water at pH = 5.5 were measured at the same observation wavelength ranges, and the global analysis of the fluorescence intensity decays were performed in the same manner as those for the parent molecules (Tyr and Tyr(Me); see Section 3.1.2, "Time-Resolved Fluorescence Spectroscopy"). The obtained results are collected in Table 3 in which the pre-exponential factors from the single-file analysis at 310 nm for the Tyr derivatives and 315 nm for Tyr(Me) are also presented. For the AcTyr derivative, the double exponential function was needed to fit to the experimental fluorescence intensity decay. The revealed fluorescence lifetimes are equal to 3.27 and 0.60 ns (from the global analysis), with a contribution of $\alpha_1 = 0.881$ and $\alpha_2 = 0.119$ (from single-file analysis), respectively (Figure 4). To the best of our knowledge, this is the first report of the biexponential fluorescence intensity decay of AcTyr. According to the literature data, the fluorescence intensity decay of AcTyr was monoexponential, with fluorescence lifetimes of $\tau = 3.2$ ns,[6] $\tau = 3.6$ ns at pH = 5.2,[4,5] $\tau = 3.27$ ns,[13] $\tau = 3.32$ ns.[45] The DAS, calculated based on the steady-state fluorescence spectrum, and obtained fractional contributions have the same shape and position as the Tyr fluorescence spectrum for both lifetimes (figure not shown). Moreover, the fluorescence lifetime decay of AcTyr(Me) is monoexponential, with a fluorescence lifetime of $\tau = 4.48$ ns, which is shorter than that of the parent molecule (4.82 ns).

The fluorescence intensity decays for the amide derivative of both Tyr and Tyr(Me) are biexponential. Moreover, the heterogeneity of the fluorescence intensity decay observed for $TyrNH_2$, expressed by the χ^2_R value obtained from the global analysis for the fit of the monoexponential function to the experimental data ($\chi^2_R = 8.67$) is greater than that for $Tyr(Me)NH_2$ ($\chi^2_R = 1.74$). The obtained result for the fluorescence decay of $TyrNH_2$ is comparable to the data obtained from the single-file analysis presented in the literature.[3,5−7,14] The DAS for both individuals associated with the long and short decay times obtained for $TyrNH_2$, as well as $Tyr(Me)NH_2$, as in the case of AcTyr, are identical (the same shape and position) to those of the parent molecules (figure not shown). A conversion of the amino group of the tyrosine amide or *O*-methyl-tyrosinamide to a *N*-acetyl derivative caused an increase of the fluorescence lifetime, compared to the amide with a protonated amino group, and simultaneously decreased the heterogeneity of the decay (see Table 3). For $AcTyrNH_2$, the χ^2_R value from the global analysis for monoexponential fit to the fluorescence intensity decay is 3 times lower than that for $TyrNH_2$; moreover, the decay still remains heterogeneous. The biexponential function with lifetimes of $\tau = 1.67$ ns and $\tau = 0.40$ ns is needed for an acceptable fit to the experimental data. The fluorescence lifetimes obtained from the global analysis are comparable to the published values.[3−5,13,43] For $AcTyr(Me)NH_2$ the reduction of heterogeneity leads to the almost-monoexponential fluorescence decay. The global χ^2_R value for the fit of the monoexpo-

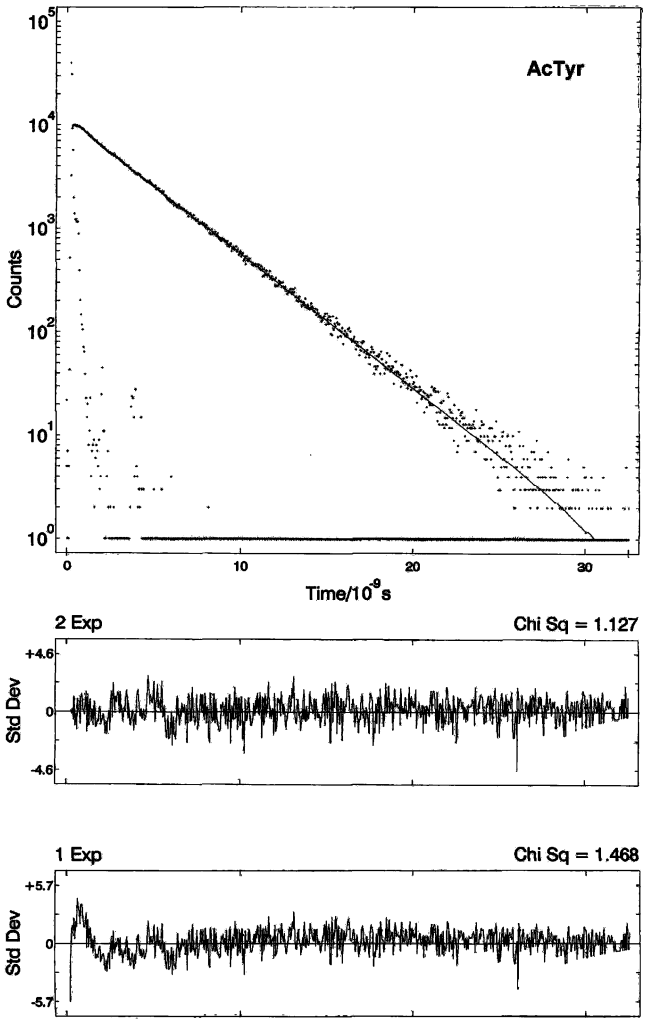

Figure 4. (- - -) Measured and (—) fitted fluorescence intensity decay versus time (left set of points represents a laser profile) of AcTyr in water at pH = 5.5. Weighted residuals for biexponential and monoexponential fits are plotted in the lower portion of the figure.

TABLE 4: Fluorescence Lifetime (τ) and Quality of Fit (χ^2_R) Obtained from Global Analysis, Pre-exponential Factor (α) Obtained from the Single-File Analysis at 315 mm, Fluorescence Rate Constant (k_f), and Nonradiative Rate Constant (k_{nr}) for Tyrosine and Its Derivatives in Acetonitrile

compound	QY	τ (ns)	α	χ^2_R	k_f ($\times 10^{-7}$ s^{-1})	k_{nr} ($\times 10^{-8}$ s^{-1})
Tyr[a]						
AcTyr	0.2	4.20 ± 0.05	1	1.07	4.69	1.91
$TyrNH_2$	0.2	4.19 ± 0.04	1	1.04	4.87	1.9
$AcTyrNH_2$	0.2	4.26 ± 0.06	1	1.06	4.79	1.87
Tyr(Me)	0.18	4.62 ± 0.07	1	1.1	3.9	1.77
AcTyr(Me)	0.19	4.74 ± 0.04	1	1.12	4	1.71
$Tyr(Me)NH_2$	0.19	4.83 ± 0.03	1	1.09	3.93	1.67
$AcTyr(Me)NH_2$	0.19	4.83 ± 0.02	1	1.09	3.93	1.67

[a] Solubility was too low for fluorescence quantum yield and lifetime measurements.

nential function is 1.26 and decreases to a value of 1.02 for the biexponential fit with lifetimes of $\tau = 2.46$ ns and $\tau = 0.66$ ns with a low (~6% in the decay) contribution of the second component (see Table 3). Thus, the hydroxyl group of a phenol ring devoid of the possibility of forming strong hydrogen-bond network with the solvent molecule(s) substantially influences the fluorescence intensity decay of the Tyr derivatives.

The fluorescence rate constants calculated based on the equation $k_f = QY/\langle\tau\rangle$ are, within the range of experimental error,

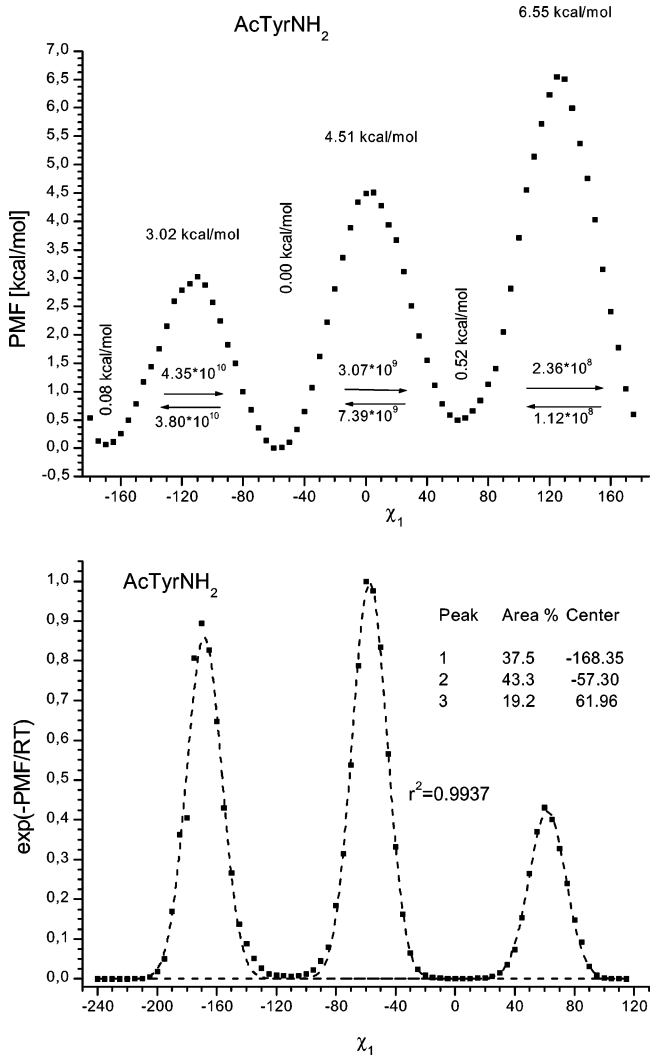

Figure 5. PMF profile (top) and rotamer probability distribution function (bottom) for $AcTyrNH_2$, each expressed as a function of the dihedral angle χ_1. The dashed line represents the best fit of the Gaussian function.

equal to ~4.1×10^7 s^{-1} and are the same for all compounds studied. Much more diversified are the nonradiative rate constants calculated from equation $k_{nr} = (1 - QY)/\tau$ (see Table 3), which indicates that the quenching process by an amide group is a dynamic process, the effectiveness of which is dependent on the distance between the chromophore and the quencher group, their mutual spatial location, and the hydration of all molecules. This quenching process can be associated with the electron (charge) transfer from the excited phenol chromophore (donor) to the amide group (acceptor), as was suggested previously.[6,7,13,17,22,60]

3.3. Photophysical Properties of Tyrosine Derivatives in Acetonitrile. To explain the influence of water on the tyrosine photophysical properties and the role of hydrogen-bond network in the modifications of photophysical properties of tyrosine and its simple derivatives, we performed time-resolved and steady-state fluorescence measurements in acetonitrile, which is a solvent with very weak proton-accepting properties.

3.3.1. Steady-State Fluorescence Spectroscopy. The presence of substituent(s) on the amino or carboxyl groups does not change the shape and position of the absorption and emission spectra of the Tyr derivatives in acetonitrile (spectra not shown). Absorption spectra of Tyr and Tyr(Me) derivatives in acetonitrile

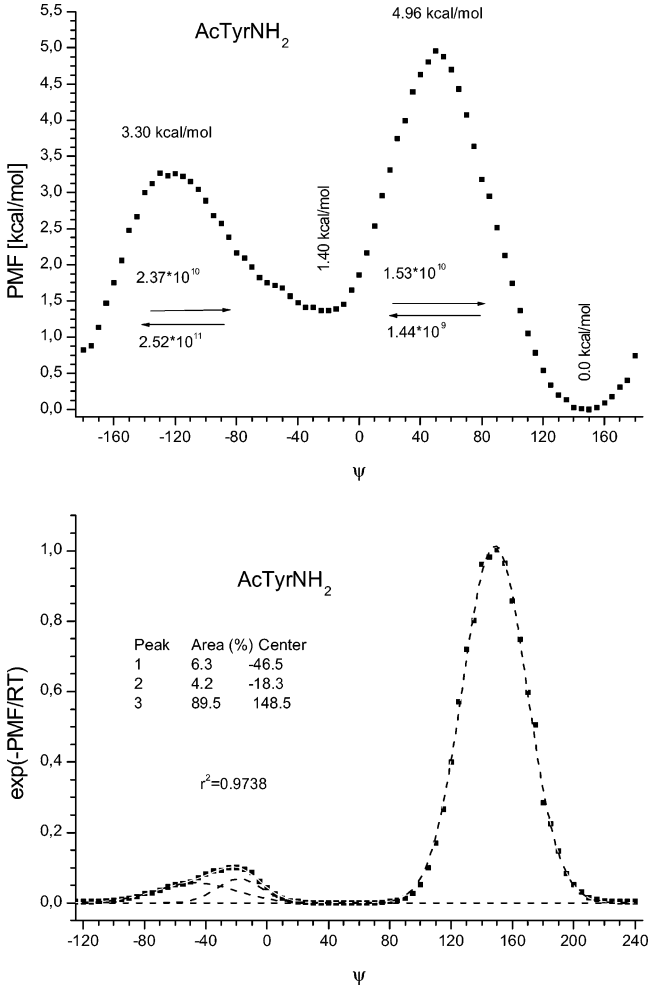

Figure 6. PMF profile (top) and rotamer probability distribution function (bottom) for $AcTyrNH_2$, each expressed as a function of the dihedral angle ψ. The dashed line represents the best fit of the Gaussian function.

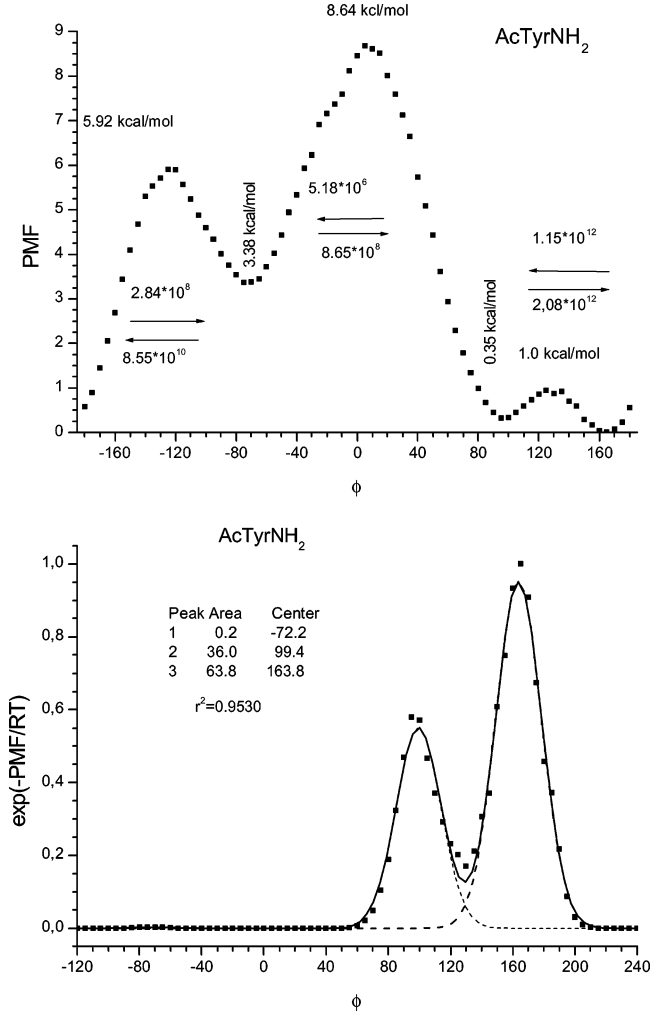

Figure 7. PMF profile (top) and rotamer probability distribution function (bottom) for $AcTyrNH_2$, each expressed as a function of the dihedral angle φ. The dashed line represents the best fit of the Gaussian function.

are red-shifted for ~4 nm, with a more-pronounced vibrational structure than in water (the absorption and emission spectra of Tyr itself could not be determined, because of its low solubility). The influence of acetonitrile on the fluorescence spectra of Tyr derivatives was less than that on the absorption spectra, causing only a small blue-shift (~1−2 nm) of fluorescence spectra. The fluorescence quantum yields of the Tyr derivatives in acetonitrile are much less diversified than those in water, except for Tyr-(Me) and AcTyr(Me) (Table 4).

3.3.2. Time-Resolved Fluorescence Spectroscopy. The fluorescence intensity decays of Tyr derivatives in acetonitrile were measured at the same observation wavelength ranges and the global analysis of the fluorescence intensity decays were performed in the same manner as for the parent molecules (Tyr and its derivatives; see Section 3.1.2, "Time-Resolved Fluorescence Spectroscopy"). The obtained results are collected in Table 4, in which the pre-exponential factors from the single-file analysis at 310 nm are also presented. For all derivatives studied, the fluorescence intensity decay is adequately described by a monoexponential function. The fluorescence lifetimes calculated from global analysis are presented in Table 4. Derivatives with free, unblocked hydroxyl groups have slightly shorter lifetimes than those of *O*-methyl tyrosine and its derivatives. This difference is probably caused by a slightly higher fluorescence rate constant calculated for tyrosine derivatives with free hydroxyl groups than the *O*-methylated ones. Contrary to the water solution for all tyrosine derivatives studied, the nonradiative rate constants are almost the same, regardless of the form of the functional group(s), which indicates that the possibility of hydrogen-bond network formation between the solvent and the phenol chromophore and amino acid moiety is very important in effective fluorescence quenching of tyrosine by the amide group.

3.4. Potential of Mean Force Calculation Results. Unrestricted MD simulations usually lead to the sampling of an energy hypersurface in the vicinity of energy minima, whereas the PMF derived by the umbrella-sampling method gives more complete information about the effective energy surface of the solute molecule. Therefore, we used PMF to estimate the changes of free energy that are associated with the rotation about the dihedral angles χ_1, χ_2, χ_3, φ, and ψ. Knowledge of the free-energy changes allows not only calculation of the rotamer populations that are associated with a given dihedral angle, but also estimation of the rotamer interconversion rate constant. For calculation, we chose tyrosine and the most satirically crowded *N*-acetyl-tyrosinamide. Sample PMF profiles and the corresponding probability distribution in χ_1, ψ, and φ for $AcTyrNH_2$ are shown in Figures 5−7, respectively, for illustration.

The difference in the free energy of rotation about the respective dihedral angles obtained from PMF calculations and the forward and backward rate constant of barrier crossing, calculated based on eqs 6 and 7, as well as the dihedral angle

TABLE 5: Energy Barrier of Rotation around the Dihedral Angle Obtained from PMF Calculation and Forward and Backward Rate Constants of Barrier Crossing, Calculated Based on eqs 6 and 7 for Tyrosine (Tyr) and *N*-Acetyl-tyrosinamide ($AcTyrN_2$) in Water

rotation on dihedral angle	PMF_{min1}		PMF_{max}		PMF_{min2}		rate constant ($\times 10^{-9}$ s^{-1})	
	value (kcal/mol)	angle (deg)	value (kcal/mol)	angle (deg)	value (kcal/mol)	angle (deg)	forward	backward
				Tyr				
	0.7	−167	3.05	−115	0.0	−55	111.2	36.1
χ_1	0.0	−55	3.42	4	0.9	55	19.3	88.5
	0.9	55	6.42	125	0.7	167	0.76	0.37
	0.0	−86	3.59	10	0.0	99	14.5	14.5
χ_2	0.0	99	3.72	179	0.0	−86	11.7	11.7
	0.0	−58	3.01	−2	0.0	54	38.7	38.7
φ	0.0	54	3.07	116	0.0	180	34.9	34.9
	0.0	180	3.03	−122	0.0	−58	37.4	37.4
	0.0	−31	2.01	−121	0.0	150	2.09	2.09
ψ	0.0	150	2.01	60	0.0	−31	2.09	2.09
	0.0	4.0	3.44	−86	0.0	183	18.7	18.7
χ_3	0.0	183	3.44	95	0.0	4.0	18.7	18.7
				$AcTyrNH_2$				
	0.08	−171	3.02	−113	0.0	−58	43.5	38.0
χ_1	0.0	−58	4.51	4	0.52	63	3.1	7.4
	0.52	63	6.55	126	0.08	−171	0.24	0.11
	0.17	−89	3.64	−6	0.0	89	18.0	13.3
χ_2	0.0	89	3.64	180	0.17	−89	13.3	18.0
	0.0	163	5.92	−123	3.38	−72	0.28	85.5
φ	3.38	−72	8.66	5	0.35	96	0.87	0.0052
	0.35	96	1.00	130	0.0	163	2100	1200
	0.0	150	3.30	−125	1.4	−23	23.7	25.2
ψ	1.4	−23	4.96	50	0.0	150	15.3	1.4
	0.0	173	3.25	−87	0.0	−2	27.1	27.1
χ_3	0.0	−2	3.25	90	0.0	173	27.1	27.1

values for appropriate rotamers for tyrosine and *N*-acetyl-tyrosinamide in water, are summarized in Table 4.

The differences between minimal and maximal values in the PMF profiles, expressed as a function of the dihedral angles χ_2 and χ_3, are ∼3.5−3.7 kcal/mol for both Tyr and $AcTyrNH_2$; thus, the rate constant of rotamer interconversion is on the order of 10^{10} s^{-1}, i.e., much higher than the fluorescence rate constant. The free-energy barrier obtained for phenol hydroxyl group rotation (∼3.3−3.4 kcal/mol; see Table 5) is comparable to that published by Hollas,[65] which indicates that the barriers of internal rotations obtained from our PMF profiles are reasonable. The correctness of the PMF profile calculation additionally supports a lack of temperature dependence, in the range of experimental error, of the χ_1 rotamer population of $AcTyrNH_2$, calculated based on ^1H NMR. For this derivative, the difference in energy of the χ_1 rotamers is in the range of 0.52 kcal/mol. As a result, the dependency of rotamer population on temperature is very weak. The barrier that is associated with the rotation of the ammonium and carboxylate group of tyrosine are ∼3 and ∼2 kcal/mol, respectively (see Table 5). For the aforementioned angle, the PMF profiles are symmetrical and a periodical function of the dihedral angle. A more-diversified profile represents the PMF in the dihedral angle χ_1 for Tyr and $AcTyrNH_2$, for which three distinct minima and three maxima with different heights are present. The highest barriers calculated for Tyr and $AcTyrNH_2$, relative to the rotation about the dihedral angle χ_1, are ∼6.5 kcal/mol, and the calculated rate constants for rotamer interconversion between rotamer populations p_{III} and p_{II} are $\sim 4 \times 10^8$ and $\sim 1 \times 10^8$ s^{-1} for Tyr and $AcTyrNH_2$, respectively. These values are almost 1 order of magnitude higher than the rate constant for radiative transition for these compounds (see Table 3). The rate constant of interconversion between rotamer populations p_{III} and p_I, as well as between rotamer populations p_I and p_{II} (and vice versa) are much higher for both tyrosine and *N*-acetyl-tyrosinamide. This conclusion agrees with the results obtained by Kungl[66] for tyrosine and tyrosine-containing peptides from MD calculations.

TABLE 6: Relative Rotamer Population (pop) and Dihedral Angle for Tyr and $AcTyrNH_2$ in Water Obtained from the Theoretical Calculations (PMF)

Tyr		$AcTyrNH_2$	
pop (%)	angle (deg)	pop (%)	angle (deg)
	χ_1, rotamer p_I		
63.6	−55.3	43.3	−57.3
	χ_1, rotamer p_{II}		
21.0	−166.2	37.5	−168.4
	χ_1, rotamer p_{III}		
15.4	55.2	19.2	62.0
	χ_2		
53.3	−85.1	42.5	−92.4
46.7	98.1	56.5	88.4
	φ		
35.0	−58.2	0.2	−72.2
32.8	53.7	36.0	99.4
32.2	180.2	63.8	163.8
	ψ		
		6.3	−46.5
49.8	−32.0	4.2	−18.3
50.2	148.2	89.5	148.5
	χ_3		
50.6	4.4	51.0	−0.5
49.4	184.5	49.0	−180.8

The rotamer populations calculated based on the PMF profile generally are comparable to those obtained from ^1H NMR spectroscopy (Table 6). The PMF calculation for tyrosine overestimates p_I and underestimates that of p_{III}, whereas, for $AcTyrNH_2$, the opposite is true. Taking into account that the error associated with NMR rotamer estimation is ∼0.05,[5] the obtained results are reasonable. Table 7 also presents the χ_1 rotamer populations for *N*-acetyl tyrosine and tyrosinamide and their *O*-methylated derivatives. For all compounds studied, three χ_1 rotamers exist in the ground state. As can be observed, the conversion of the hydroxyl group to the methoxy group does

TABLE 7: χ_1 Rotamer Populations (p_i) for Tyrosine and Its Derivatives in Water, Calculated Based on ^{1}H NMR Spectroscopy

compound	p_I	p_{II}	p_{III}
Tyr	0.43;[a] 0.49;[b] 0.49;[c] 0.48	0.24;[a] 0.26;[b] 0.21;[c] 0.25	0.33;[a] 0.25;[b] 0.30;[c] 0.27
Tyr(Me)	0.43;[b] 0.48	0.29;[b] 0.25	0.25;[b] 0.27
AcTyr	0.60;[b] 0.57	0.24;[b] 0.25	0.16;[b] 0.18
AcTyr(Me)	0.57	0.25	0.18
$TyrNH_2$	0.45; 0.46[b]	0.38; 0.37[b]	0.17; 0.17[b]
$Tyr(Me)NH_2$	0.43	0.39	0.18
$AcTyrNH_2$	0.58;[b] 0.56	0.32;[b] 0.32	0.10;[b] 0.12
$AcTyr(Me)NH_2$	0.59	0.32	0.09

[a] Data from ref 68. [b] Data from ref 5. [c] Data from ref 69.

not have any influence on the rotamer populations. The conversion of the carboxylate into the amide group increases the population p_{II} at the expense of p_{III}, whereas the acetylation of the ammonium group causes an increase of p_I and a decrease of that of p_{III}, as compared to Tyr, but the changes are not as large.

The rate constant of rotamer interconversion associated with the rotation about the dihedral angle ψ for $AcTyrNH_2$ is higher than the rate constant of radiative transition calculated based on the fluorescence quantum yield and the fluorescence lifetime. The PMF profile, expressed as a function of ψ (rotation of the amide group), possesses three minima (at $-47°$, $-18°$, and $149°$) and two maxima (at $-120°$ (3.30 kcal/mol) and $\sim 40°$ (5 kcal/mol)) (see Figure 6 and Table 4). The calculated rotamer probability distribution function reveals the presence of three rotamers: one centered at $149°$, with a population of $\sim 90\%$, and two weakly resolved rotamers, at $-47°$ and $-18°$, with populations of 6% and 4%, respectively. The slowest rotamer interconversion rate constant is $\sim 10^9\ s^{-1}$, i.e., much higher than the radiative rate constant obtained for $AcTyrNH_2$. Thus, during the excited-state lifetime, the amide group can rotate significantly. All presented results indicate that the entire amino acid moiety (rotation by the dihedral angle χ_1), as well as the amide group in particular (rotation by the dihedral angle ψ), can rotate, with the rate constant being higher than the fluorescence rate constant. Taking into account that the χ_1 rotamer populations for all compounds studied are similar, it can be assumed that, for AcTyr and $TyrNH_2$, for which the PMF profile was not studied, the rate constant of χ_1 rotamer interconversion is at least of the same order of magnitude as that for $AcTyrNH_2$. The exception is the rotation of the acetyl group in $AcTyrNH_2$, for which the highest energy barrier (8.6 kcal/mol) and the smallest interconversion rate constant between two rotamers were obtained ($5.2 \times 10^6\ s^{-1}$; see Table 5 and Figure 7). Thus, the acetyl group cannot freely rotate but only vibrate in the range of $\sim 120°$, which is associated with the presence of two rotamers: $p_I = 36\%$ (centered at $99°$) and $p_{II} = 64\%$ (centered at $163.5°$) (see Figure 7). However, the acetyl group exerts a small quenching effect and only a biexponential fluorescence intensity decay of AcTyr can be associated with hindered rotation of this group. Thus, the heterogeneous χ_1 rotamer population in the ground state cannot be responsible for the heterogeneous fluorescence intensity decay of tyrosinamide and its derivatives.

4. Conclusions

The global analysis of the fluorescence intensity decays of tyrosine (Tyr) and *O*-methyl tyrosine (Tyr(Me)) has revealed that the hydroxyl group of the phenol chromophore interacts with water molecules, resulting in very weak long-wave fluorescence, similar to that observed for Tyr fluorescence in a buffer solution containing a strong hydrogen acceptor. The replacement of the amino group in tyrosine by the acetyl group causes a decrease of the fluorescence quantum yield, as observed previously, whereas the fluorescence lifetime is biexponential, with a small contribution from a subnanosecond component. The acetyl group also quenches the *N*-acetyl-*O*-methyl-tyrosine (AcTyr(Me)) fluorescence; however, monoexponential fluorescence intensity decay is observed for *N*-acetyl tyrosine with blocked hydroxyl groups, beside stronger quenching than that observed for AcTyr. This indicates that the heterogeneous fluorescence intensity decay observed for AcTyr and other Tyr derivatives is probably caused by specific hydration of the acetyl (the entire amino acid moiety) and hydroxyl groups by solvent molecules, forming a hydrogen-bond network, and solvent reorientation is, possibly, also an important factor in the quenching.[58] The global analysis of the fluorescence intensity decays of tyrosinamide with blocked or free amino or/and hydroxy groups conforms with the earlier finding,[3−6,13,19,21,22,60,61] that the amide group is a strong Tyr quencher, regardless of the form of the amino or the hydroxy group (blocked or free). Monoexponential fluorescence intensity decays of Tyr derivatives and the lack of quenching by an amide group in acetonitrile strongly support an important role of the hydrogen-bond network in the Tyr fluorescence quenching process by electron transfer from an excited phenol chromophore to an amide group. The potential of mean force (PMF) calculations indicate that the ground-state heterogeneous χ_1 rotamer population in water, assuming $\kappa = 1$ in eq 9, is not responsible for the biexponential fluorescence intensity decays of the Tyr derivatives, because of the high estimated rate constant of rotamer interconversion, which is higher than the radiative rate constant. However, the exact value of κ is unknown, and a hydrogen-bond network or other currently unknown factor can increase friction (or the barrier) to slow the rotation, so it can affect the fluorescence. Our results are in agreement with the findings of Lakowicz,[67] that spectral relaxation rather than the rotamer seems to be a significant, if not dominant, source of heterogeneous fluorescence intensity decay in single tryptophan proteins.

Acknowledgment. This work was supported by the State Committee for Scientific Research (KBN), under Grant No. 0369/T09/98/15.

References and Notes

(1) Beechem, J. M.; Brand, L. *Annu. Rev. Biochem.* **1985**, *54*, 43−71.
(2) Eftink, M. R. In *Protein Structure Determination*; Schulter, C. H., Ed.; Methods of Biochemical Analysis, Vol. 35; Wiley: New York, 1991.
(3) Ross, J. B. A.; Laws, W. R.; Rousslang, K. W.; Wyssbrod, H. R. In *Biochemical Applications*; Lakowicz, J. R., Ed.; Topics in Fluorescence Spectroscopy, Vol. 3; Plenum Press: New York, 1992; pp 1−63.
(4) Ross, J. B. A.; Laws, W. R.; Sutherland, J. C.; Buku, A.; Katsoyannis, P. G.; Schwartz, I. L.; Wyssbrod, H. R. *Photochem. Photobiol.* **1986**, *44*, 365−370.
(5) Laws, W. R.; Ross, J. B. A.; Wyssbrod, H. R.; Beechem, J. M.; Brand, L.; Sutherland, J. C. *Biochemistry* **1986**, *25*, 599−607.
(6) Gauduchon, P.; Whal, P. *Biophys. Chem.* **1978**, *8*, 87−104.
(7) Wiczk, W.; Rzeska, A.; Łukomska, J.; Stachowiak, K.; Karolczak, J.; Malicka, J.; Łankiewicz, L. *Chem. Phys. Lett.* **2001**, *341*, 99−106.

(8) Guzow, K.; Szabelski, M.; Rzeska, A.; Karolczak, J.; Sulowska, H.; Wiczk, W. *Chem. Phys. Lett.* **2002**, *362*, 519−526.
(9) Rayner, D. M.; Szabo, A. G. *Can. J. Chem*. **1978**, *56*, 743−745.
(10) Rayner, D. M.; Szabo, A. G. *J. Am. Chem. Soc.* **1980**, *102*, 554−563.
(11) Engh, R. A.; Chen, L. X.-Q.; Fleming, G. R. *Chem. Phys. Lett*. **1986**, *126*, 365−372.
(12) Gordon, H. R.; Jarrell, H. C.; Szabo, A. G.; Willis, K. J.; Somorjai, R. L. *J. Phys. Chem.* **1992**, *96*, 1915−1921.
(13) Seidel, C.; Orth, A.; Greulich, R. O. *Photochem. Photobiol*. **1993**, *58*, 178−184.
(14) Łukomska, J.; Rzeska, A.; Malicka, J.; Wiczk, W. *J. Photochem. Photobiol., A: Chem*. **2001**, *142*, 135−139.
(15) Cowgill, R. W. *Biochim. Biophys. Acta* **1967**, *133*, 6−18.
(16) Cowgill, R. W. *Arch. Biochem. Biophys.* **1963**, *100*, 36−44.
(17) Tournon, J. E.; Kuntz, E.; El Bayoumi, M. A. *Photochem. Photobiol.* **1972**, 16, 425−433.
(18) Feitelson, J. *J. Phys. Chem.* **1964**, *68*, 391−397.
(19) Wiczk, W.; Łankiewicz, L.; Czaplewski, C.; Ołdziej, S.; Stachowiak, K.; Michniewicz, A.; Micewicz, B.; Liwo, A. *J. Fluoresc.* **1997**, *7*, 257−266.
(20) Wiczk, W.; Łankiewicz, L.; Czaplewski, C.; Ołdziej, S.; Stachowiak, K.; Michniewicz, A.; Liwo, A. *J. Photochem. Photobiol., A: Chem.* **1996**, *101*, 171−181.
(21) Wiczk, W.; Stachowiak, K.; Czaplewski, C.; Łankiewicz, L.; Michniewicz, A. *J. Photochem. Photobiol., A: Chem.* **1997**, *102*, 189−195.
(22) Wiczk, W.; Stachowiak, K.; Skurski, P.; Łankiewicz, L.; Michniewicz, A.; Rój, A. *J. Am. Chem. Soc.* **1996**, *118*, 8300−8307.
(23) Giancotti, V.; Quadrifoglio, F.; Cowgill, R. W.; Crane-Robinson, C. *Biochim. Biophys. Acta* **1980**, *624*, 60−65.
(24) Giancotti, V.; Fonda, M.; Crane-Robinson, C. *Biophys. Chem.* **1977**, *6*, 379−383.
(25) Guardia, E.; Rey, R.; Padró, J. A. *J. Chem. Phys*. **1991**, *95*, 2823−2831.
(26) Kumar, S.; Bouzida, D.; Swendsen, R. H.; Kollman, P. A.; Rosenberg, J. M. *J. Comput. Chem.* **1992**, *13*, 1011−1021.
(27) Kumar, S.; Rosenberg, J. M.; Bouzida, D.; Swendsen, R. H.; Kollman, P. A. *J. Comput. Chem.* **1995**, *16*, 1339−1350.
(28) Czaplewski, C.; Rodziewicz-Motowidło, S.; Liwo, A.; Ripoll, D. R.; Wawak, J. R.; Scheraga, H. A. *Protein Sci.* **2000**, *9*, 1235−1245.
(29) Masunov, A.; Lazardis, T. *J. Am. Chem. Soc.* **2002**, *125*, 1722−1730.
(30) Bodansky, M.; Bodansky, A. *The Practice of Peptide Synthesis*; Springer−Verlag: Berlin, Heidelberg, New York, Tokyo, 1984.
(31) Chen, R. F. *Anal. Lett.* **1967**, *1*, 35−42.
(32) Karolczak, J.; Komar, D.; Kubicki, J.; Wróżowa, T.; Dobek, K.; Ciesielska, B.; Maciejewski, A. *Chem. Phys. Lett*. **2001**, *344*, 154−164.
(33) Knutson, R. J.; Bechem, J. M.; Brand, L. *Chem. Phys. Lett.* **1983**, *102*, 501−507.
(34) Beechem, J. M.; Gratton, E.; Ameloot, M.; Knutson, R. J.; Brand, L. In *Principles*; Lakowicz, J. R., Ed.; Topics in Fluorescence Spectroscopy, Vol. 2; Plenum Press: New York, 1991; pp 241−305.
(35) Knutson, R. J.; Waldbridge, D. G.; Brand, L. *Biochemistry* **1982**, *21*, 4671−4679.
(36) Willis, K. J.; Szabo, A. G.; Drew, J.; Zuker, M.; Ridgewey, J. M. *Biophys. J.* **1990**, *57*, 183−189.
(37) Torrie, G. M.; Valleau, J. P. *J. Comput. Phys.* **1977**, *23*, 187−199.
(38) Frenkel, D.; Smit, B. *Understanding Molecular Simulation−From Algorithms to Applications*; Academic Press: San Diego, CA, 1996; Chapter 7, pp 176−181.
(39) Case, D. A.; Pearlman, D. A.; Caldwell, J. W.; Cheatham, T. E., III.; Ross, W. S.; Sim-Merling, C. L.; Darden, T. A.; Merz, K. M.; Stanton, R. V.; Cheng, A. L.; Vincent, J. J.; Crowley, M.; Ferguson, D. M.; Radmer, R. J.; Seibel, G. L.; Singh, U. C.; Weiner, P. K.; Kollman, P. A. *AMBER 5*; University of California: San Francisco, 1997.
(40) Jorgensen, W. L.; Chandrasekhar, J.; Madura, J. D.; Impey, R. W.; Klein, M. L. *J. Chem. Phys.* **1983**, *79*, 926−935.
(41) Jorgensen, W. L.; Tirado-Rives, J. J. *J. Am. Chem. Soc*. **1988**, *110*, 1666−1671.
(42) Kuharski, R. A.; Chandler, D.; Montgomery J. A., Jr.; Rabii, F.; Singer, S. J. *J. Phys. Chem.* **1988**, *92*, 3261−3267.
(43) Lakowicz, J. R.; Laczko, G.; Gryczynski, I. *Biochemistry* **1987**, *26*, 82−90.
(44) Harms, G. S.; Paulus, S. W.; Hendstrom, J. F.; Johnson, C. K. *J. Fluoresc.* **1997**, *7*, 283−292.
(45) Pal, H.; Palit, D. K.; Mukherjee, D.; Mittal, J. P. *J. Photochem. Photobiol., A: Chem.* **1990**, *52*, 391−409.
(46) Bhatnagar, G. M.; Grunen, L. C.; Maclaren, J. A. *Aust. J. Chem.* **1968**, *21*, 3005−3013.
(47) Rayner, D. M.; Krajcarski, D. T.; Szabo, A. G. *Can. J. Chem.* **1977**, *56*, 1238−1245.
(48) Shimizu, O.; Imakubo, K. *Photochem. Photobiol.* **1977**, *26*, 541−543.
(49) Schnarr, M.; Helene, C. *Photochem. Photobiol*. **1982**, *36*, 91−93.
(50) Willis, J. K.; Szabo, A. G. *J. Phys. Chem*. **1991**, *95*, 1585−1589.
(51) Lee, J. K.; Ross, R. T.; Thampi, S.; Leurgans, S. *J. Phys. Chem*. **1992**, *96*, 9158−9162.
(52) Lee, J. K.; Ross, R. T. *J. Phys. Chem. B* **1998**, *102*, 4612−4618.
(53) Harms, G. S.; Paulus, S. W.; Hendstrom, J. F.; Johnson, C. K. *J. Fluoresc*. **1997**, *7*, 273−282.
(54) Ferreira, S. T.; Stella, L.; Gratton, E. *Biophys. J*. **1994**, *66*, 1185−1196.
(55) Willis, K. J.; Szabo, A. G.; Krajcarski, D. T. *Photochem. Photobiol*. **1990**, *51*, 375−377.
(56) Creed, D. *Photochem. Photobiol*. **1984**, *39*, 563−575.
(57) Mahomoud, S. F.; Bialkowski, S. E. *Appl. Spectrosc*. **1995**, *49*, 1669−1676.
(58) McCurie, R.; Feldman, I. *Photochem. Photobiol*. **1973**, *18*, 119−124.
(59) Contino, P. B.; Laws, W. R. *J. Fluoresc.* **1991**, *1*, 5−13.
(60) Schwartzwald, R.; Seidel, C.; Goody, R. S.; Kuhn, P. K.; Greulich, K. O. *Ber. Bunsen−Ges. Phys. Chem*. **1989**, *93*, 342−346.
(61) Edelhogh, H.; Perlman, R. L.; Wilchek, M. *Biochemistry* **1968**, *7*, 3839−3900.
(62) Fraggi, M.; DeFelippis, M. R.; Klapper, M. H. *J. Am. Chem. Soc*. **1989**, *111*, 5141−5145.
(63) Cowgill, R. In *Biochemical Fluorescence*; Chen, R. F., Edehoch, H., Eds.; Marcel Dekker: New York and Basel, Switzerland, 1976; Chapter 9.
(64) Szabelski, M.; Guzow, K.; Rzeska, A.; Malicka, J.; Przyborowska, M.; Wiczk, W. *J. Photochem. Photobiol., A: Chem*. **2002**, *152*, 73−78.
(65) Hollas, J. M. *Modern Spectroscopy*, 2nd ed.; Wiley: Chichester, U.K., 1992; p 180.
(66) Kungl, A. *J. Biophys. Chem*. **1992**, *45*, 41−50.
(67) Lakowicz, J. R. *Photochem. Photobiol.* **2000**, 72, 421−437.
(68) Cavanaugh, J. R. *J. Am. Chem. Soc*. **1970**, *93*, 1488−1493.
(69) Kainosho, M.; Ajisaka, K. *J. Am. Chem. Soc*. **1975**, *97*, 5630−5631.